Analysis of the 1957 Andreanof Islands Earthquake
14-08-0001-G1766

Thomas M. Boyd
Colorado School of Mines
Department of Geophysics
Golden, CO 80401
(303) 273-3522

Project Summary and Goals

Recent studies have indicated that the spatial distribution of moment release can be quite heterogeneous along any particular rupture zone. The most common explanation for this heterogeneity has been the rupture of strong patches, or asperities, along the fault plane [e.g., Ruff and Kanamori, 1983]. These strong patches could arise from spatial variations of the frictional characteristics along the fault or from geometrical barriers inherent to the fault's shape. Alternatively, the spatial distribution of moment release could have little to do with the physical characteristics of the fault's surface and may be related to the dynamics of slip and how regions of the fault interact with neighboring regions [e.g., Rundle and Kanamori, 1987; Horowitz and Ruina, 1989].

Distinctions between these two models can not be made from the analysis of single events [e.g., Thatcher, 1990]. Conclusive observations can only be drawn from a study of the moment-release distribution generated by several great earthquakes, all of which rupture the same fault segment. In this context, an excellent region of study is the central Aleutian Arc. In 1986, a magnitude 8.0 (M_W) earthquake occurred near the Andreanof Islands. Its slip distribution, aftershock, and preshock sequence have been described in detail in a number of recent studies. Prior to 1986, the central Aleutian Arc was ruptured by another great earthquake in 1957 ($M_W > 8.5$). The 1957 Andreanof Islands earthquake, however, remains poorly understood. Its seismic moment, slip distribution, and rupture area have not been well constrained.

The short time span between the 1957 and 1986 earthquakes provides us with a unique opportunity to study a complete seismic cycle bounded by two instrumentally recorded great earthquakes. In fact, it represents the only complete seismic cycle instrumentally observed along the Aleutian Arc. As briefly described in this summary, we are continuing our work on assembling and interpreting observations pertinent to the 1957 earthquake and the interseismic period between the 1957 and 1986 events. Progress can be summarized as;

1) We have developed and applied a methodology for assessing confidence bounds on rupture lengths constrained using surface-wave directivities.

2) Page scanning and relocation of seismicity listed in both the *BCIS* and *ISS* for the years 1957 thru 1989 continues.

3) Source mechanisms for aftershocks of the 1957 event have been classified by event type (thrust, normal, etc.), and bodywave modeling of selected events has begun.

Rupture Length Estimates and Error Bounds

Accurate determinations of kinematic rupture parameters have been accomplished for some time using the so-called directivity function [e.g., Ben-Menahem, 1961; Ben-Menahem and Toksoz, 1962, 1963; Udias, 1971]. Unfortunately, because it is highly nonlinear, this function is difficult to invert. Using the simulated annealing method [Kirkpatrick et al., 1983], however, we have constructed an inversion process which is capable of extracting accurate estimates of kinematic rupture parameters and provides the probability distribution of their values.

A PhD. level graduate student supported by this project, David Lane, has developed an ensemble approach in which several independent inversions are run simultaneously. The objective of each inversion is to maximize the joint probability distribution $P(\mathbf{M}=m|\mathbf{D}=d)$, where **M** represents the kinematic rupture parameters, and **D** represents the observed data. After several iterations the algorithm generates solutions distributed as $exp(-E/kT_j)$, where E represents the error between a possible solution and the observed data, and T_j is the control parameter of the *jth* inversion. We contend that the maximum likelihood estimate obtained during a single inversion is less important than the marginal distribution of rupture parameters. Since each of the inversions are independent we obtain the marginal distributions $P(M_i=n)$ by summing over the joint inversions. Figure 1 shows inversion results for the 1957 event using data recorded at Pietermaritzburg South Africa. We find that the observed directivity can be best modeled with bilateral source that ruptured 300 km to the west, 615 km to the east, at a velocity of about 1.5 km/s. Preliminary results from this portion of the project were presented at the 1990 Fall AGU meeting in San Francisco [Lane and Boyd, 1990]. An overview of the technique and its applications to other historically significant earthquakes will be presented at the 1991 Spring AGU meeting [Boyd et al., 1991].

Seismicity Relocations

Using the slab geometry described by Boyd and Creager [1991] and Creager and Boyd [1991] we have calculated *P-wave* travel-time perturbations to approximately 550 stations as a function of epicentral position. The calculated residuals are used directly as epicentrally varying station corrections to generate relocated epicenters without additional ray tracing. We are using this procedure to relocate all of the shallow seismicity (*BCIS* and *ISS*) that occurred between 160 W and 175 E longitude from the years 1957 through 1989.

Figure 2 shows our relocations of the earthquake activity recorded during the year 1957. Figure 3 shows space-time plots of the same seismicity distribution. From our relocations it appears as though the aftershock sequence can be divided into three temporal units. During the first, lasting about 2.2 days after the mainshock, aftershock activity is generally confined to the rupture zone defined from the surface-wave directivities described above. During the second time period (2.2 to 47 days after the mainshock) activity expands eastward to fill the Unalaska seismic gap. Activity within this portion of the aftershock zone, although low level, is persistent throughout the rest of 1957. After 47 days of activity, seismicity expands westward to include the Rat block.

During the next few months we will continue to relocate earthquakes along the central Aleutian Arc up through and beyond the occurrence of the 1986 event. Travel-time observations for the period between 1958 and 1962 do not exist in computer readable format and will be optically scanned. An undergraduate research assistant will be working full time during the summer of 1991 to complete this task. As such, we expect to complete our relocation effort early in the fall of 1991. Preliminary results from this portion of the project were presented at the 1990 Fall AGU meeting [Boyd et al., 1990].

Aftershock Source Mechanisms

Using *P-wave* first motion and *S-wave* polarization observations we have been able to classify 52 of the 92 relocated *ISS* events that occurred in 1957 by source type. Our scheme has three classifications: 1) thrust faulting, 2) normal faulting, and 3) *P-wave* first motions and *S-wave* polarizations spatially consistent, but inconsistent with either 1 or 2.

Figure 4 shows several examples of the events grouped into classes 1 and 2. All of the events identified as normal faulting earthquakes are located within or near the trench. Those identified as thrust faulting earthquakes are located along the main thrust-zone. 43 of the 92 events are in categories 1 and 2. Figure 5 shows preliminary waveform models for two such events.

Figure 6 includes several examples of earthquakes grouped into class 3. Of the 92 events, 9 fall within this category. Notice that all of these events display remarkably consistent *P* and *S-wave* observations that do not appear to be consistent with the thrust or normal faulting events one would typically find along the Aleutian Arc. To illustrate how we will determine source parameters for these events consider the earthquake shown in Figure 7. The top portion of the figure shows the location and raw first motion and *S-wave* polarization observations. Although the first motion data is relatively inconsistent, the *S-wave* polarization data is spatially consistent, but not with what would be expected for a typical, thrust faulting earthquake. The only consistent feature in the *P-wave* first motion data is the dilatational field almost due east of the epicenter. Using the *S-wave* polarization data and constraining the mechanisms to not violate the consistent feature in the *P-wave* first motion data described above, we use the formalism presented by Dillinger et al. [1971] to determine acceptable bounds on the *P* and *T* axes of the solution. The mechanism to the left shows solutions which span a 90% confidence bound on the positions of the *P* and *T* axes. Using these constraints, we then invert several waveforms to derive the final solution shown on the right. This event appears to have occurred on a high-angle normal fault within the descending slab. Preliminary results of this portion of the project will be presented along with updates on other aspects of the project at the 1991 Fall AGU meeting.

References

Ben-Menahem, A., and M. N. Toksoz, Source mechanism from spectra of long-period seismic surface waves, 1. The Mongolian earthquake of December 4, 1957. *J. Geophys. Res., 67,* 1943-1955, 1962.

Ben-Menahem, A., and M. N. Toksoz, Source mechanism form spectra of long-period surface waves, 2. The Kamchatka earthquake of November 4, 1952, *J. Geophys. Res., 68,* 5207-5222, 1963.

Boyd, T. M., and K. C. Creager, The geometry of Aleutian subduction: Three-dimensional seismic imaging, *J. Geophys. Res., 96,* 2267-2291, 1991.

Boyd, T. M., E. R. Endgahl, and W. Spence, Aftershocks of the 1957 Aleutian Islands earthquake, *EOS, 71,* 1469, 1990.

Boyd, T. M., F. D. Lane, and E. R. Engdahl, Historical earthquakes: Rupture length estimates based on aftershock locations and surface wave observations, Abstract, *EOS, 72,* 189, 1991.

Creager, K. C., and T. M. Boyd, The geometry of Aleutian subduction: Three-dimensional kinematicflow model, *J. Geophys. Res., 96,* 2293-2307, 1991.

Dillinger, W. H., A. J. Pope, and S. T. Harding, The determination of focal mechanisms using *P*- and *S-wave* data, *NOAA Tech. Report NOS 44,* 56 pp., 1971.

Horowitz, F. G., and A Ruina, Slip patterns in a spatially homogeneous fault model, *J. Geophys. Res., 94,* 10,279-10,298, 1989.

Kirkpatrick, S., C. D. Gelatt, and M. P. Vecchi, Optimization by simulated annealing, *Science, 220,* 671-680, 1983.

Lane, F. D., and T. M. Boyd, A simulated annealing approach to the inversion of surface wave directivities: Application to the 1957 Aleutian Islands earthquake, *EOS, 71,* 1468, 1990.

Ruff, L., and H. Kanamori, The rupture process and asperity distribution of three great earthquakes from long-period diffracted P-waves, *Phys. Earthq and Planet. Inter., 31,* 202-230, 1983.

Rundle, J. B., and H. Kanamori, Application of an inhomogeneous stress (patch) model to complex subduction zone earthquakes: A discrete interaction matrix approach, *J. Geophys. Res., 92,* 2606-2616, 1987.

Stauder, W., and A. Udias, S-wave studies of earthquake of the North Pacific, Part II: Aleutian Islands, *Bull. Seismol. Soc. Am., 53,* 59-77, 1963.

Thatcher, W., Order and diversity in the modes of Circum-Pacific earthquakerecurrence, *J. Geophys. Res., 95,* 2609-2624, 1990.

Udias, A., Source parameters of earthquakes from spectra of Rayleigh waves, *Geophys. J. R. Astr. Soc., 22,* 353-376, 1971.

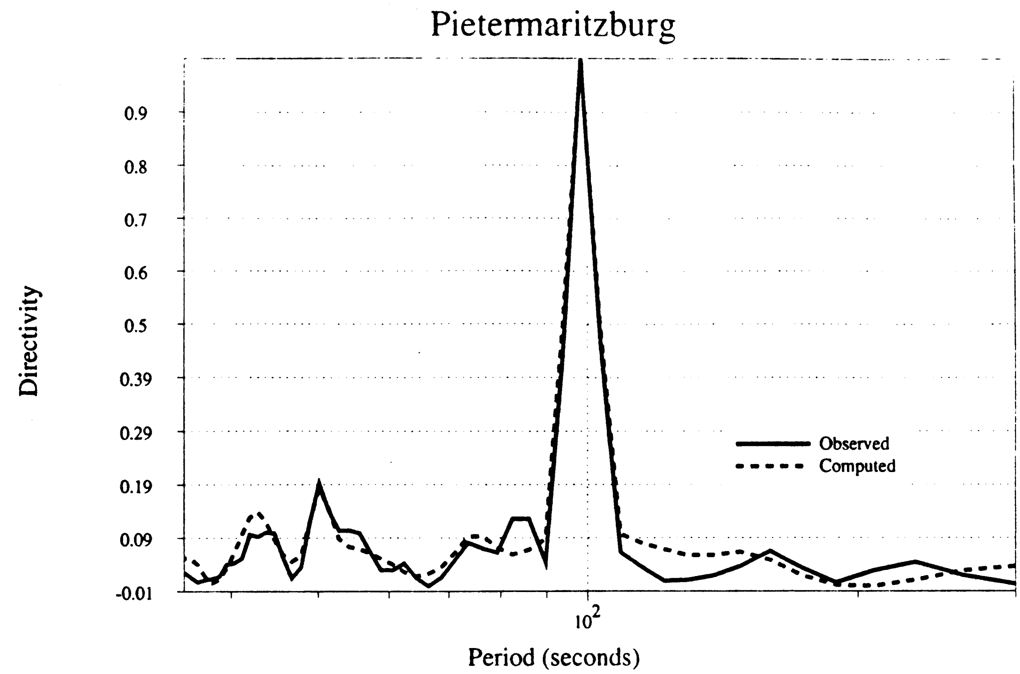

Figure 1: Normalized surface-wave directivity functions for the 1957 Andreanof Islands earthquake as observed at Pietermaritzburg South Africa. Solid lines are the observed directivities, dashed are those calcuated using the parameters described in the text.

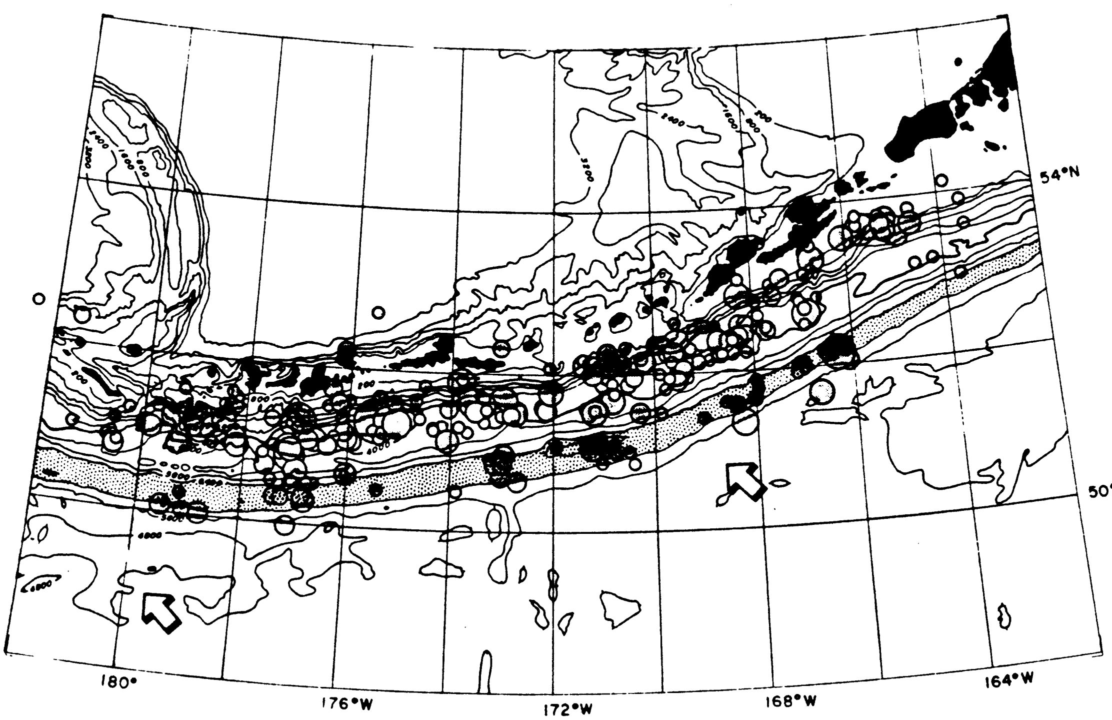

Figure 2: Aftershock relocations for events listed in both the *ISS* and *BCIS* bulletins during the calendar year 1957.

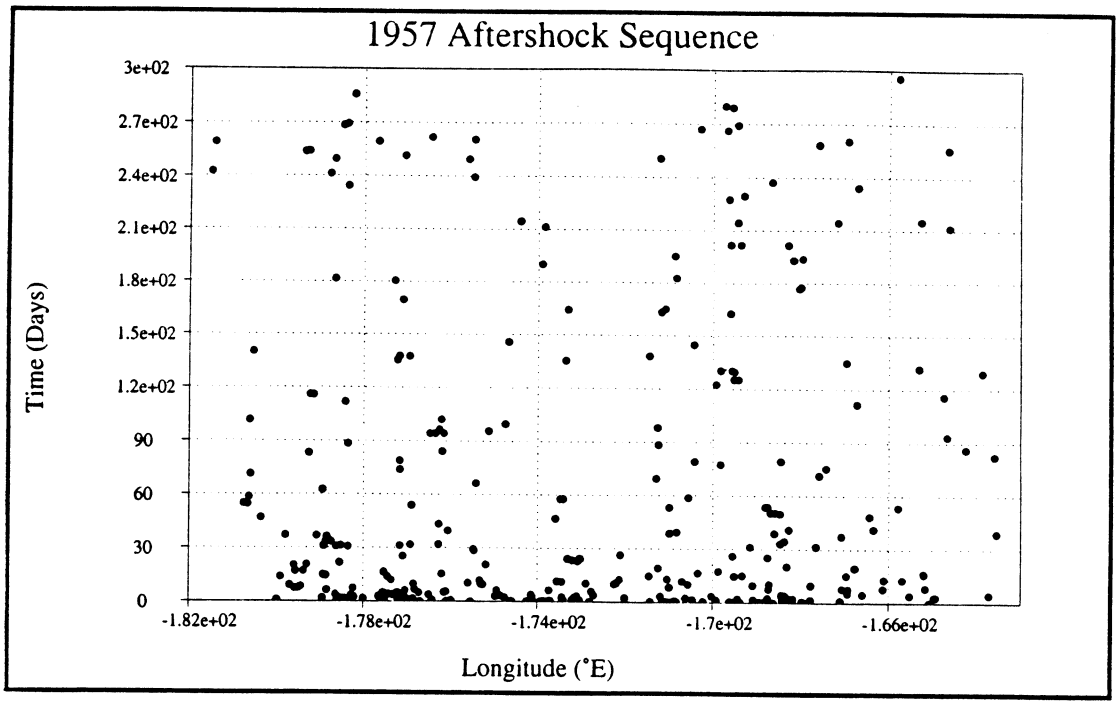

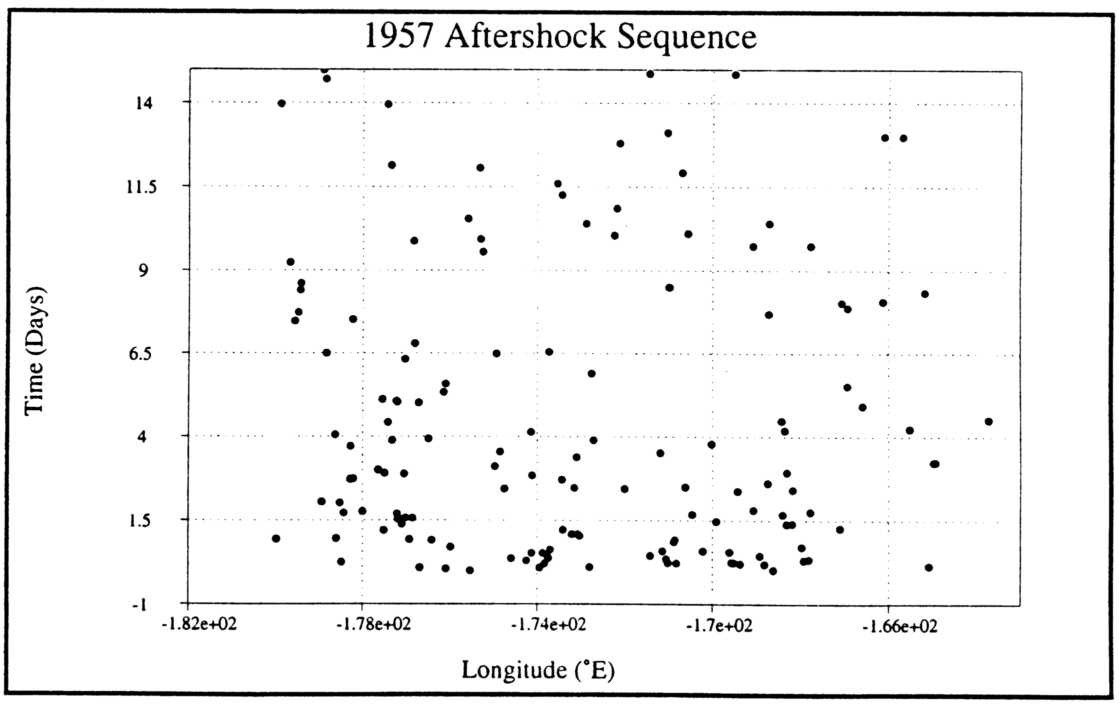

Figure 3: Space-time plots of the 1957 aftershock sequence. Top figure is for the calendar year 1957, bottom figure shows the first 15 days of the sequence.

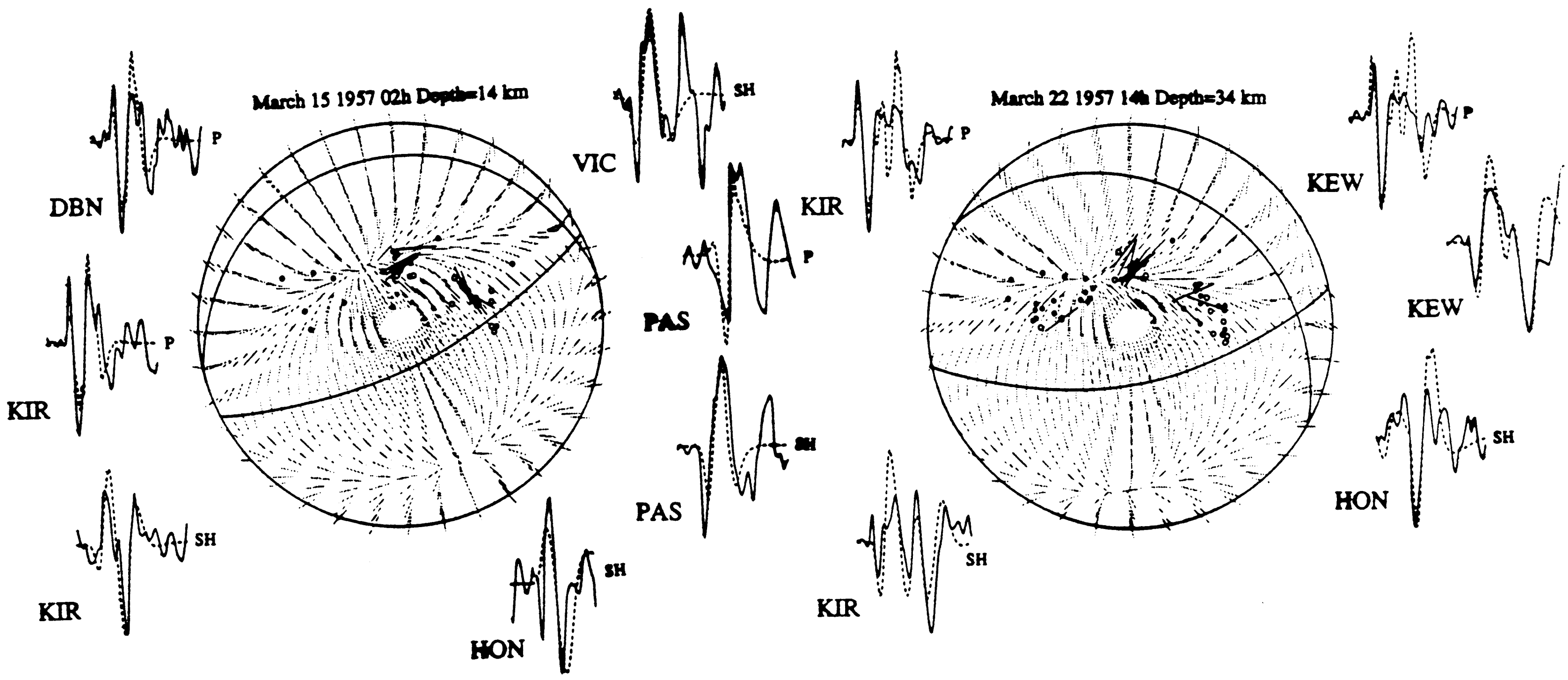

Figure 4: First motion (*ISS*) and *S-wave* polarization observations [Stauder and Udias, 1963] for events that appear to be either thrust faulting or normal faulting earthquakes. Closed circles are compressional first arrivals, open circles are dilatational first arrivals. Source mechanisms shown are those that would be expected for typical interplate thrust earthquakes.

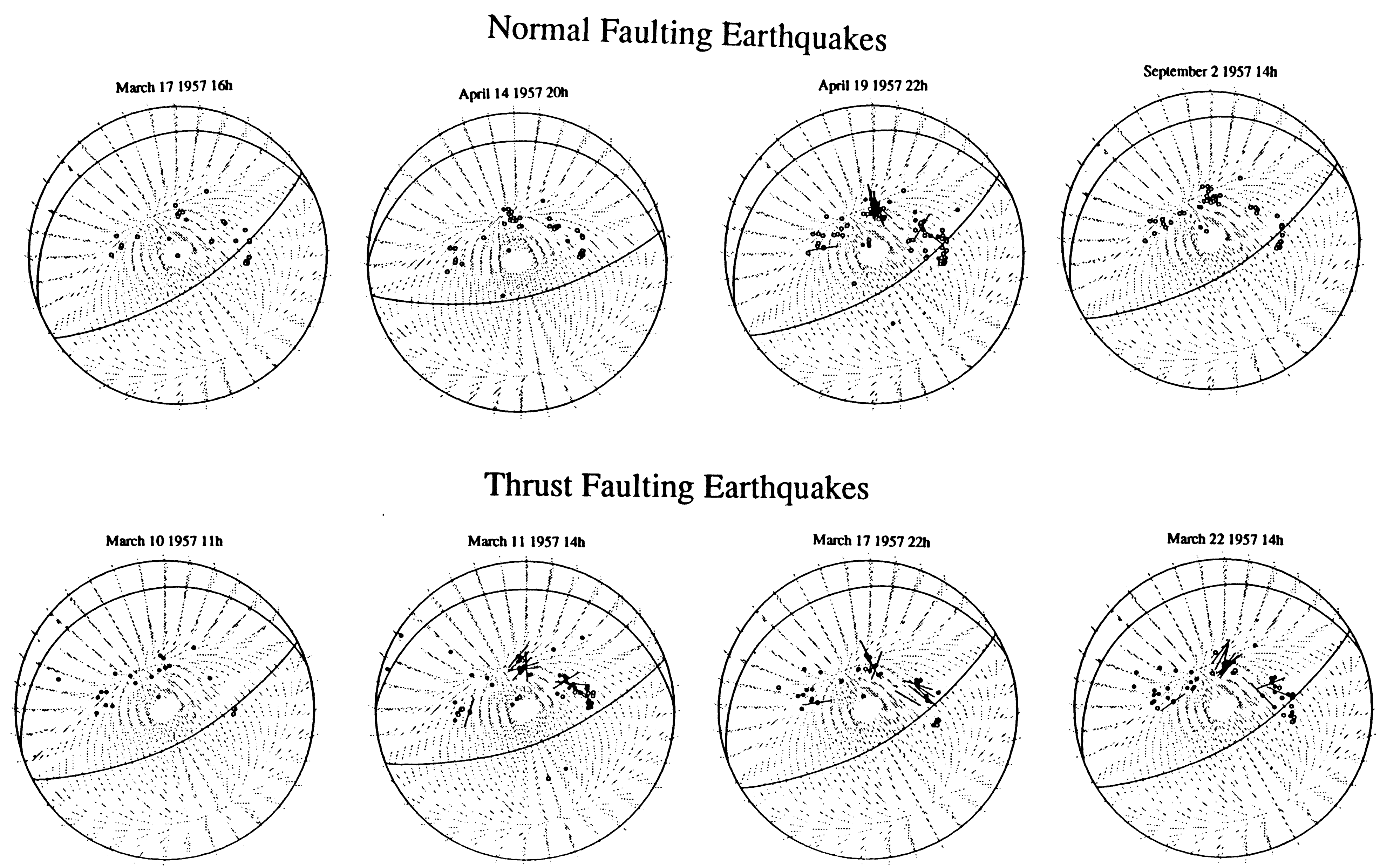

Figure 5: Source mechanisms inferred from *P-wave* first motion, *S-wave* polarization, and waveform matching. Observed waveforms are solid, synthetics are dashed. All other symbols are as defined in Figure 4.

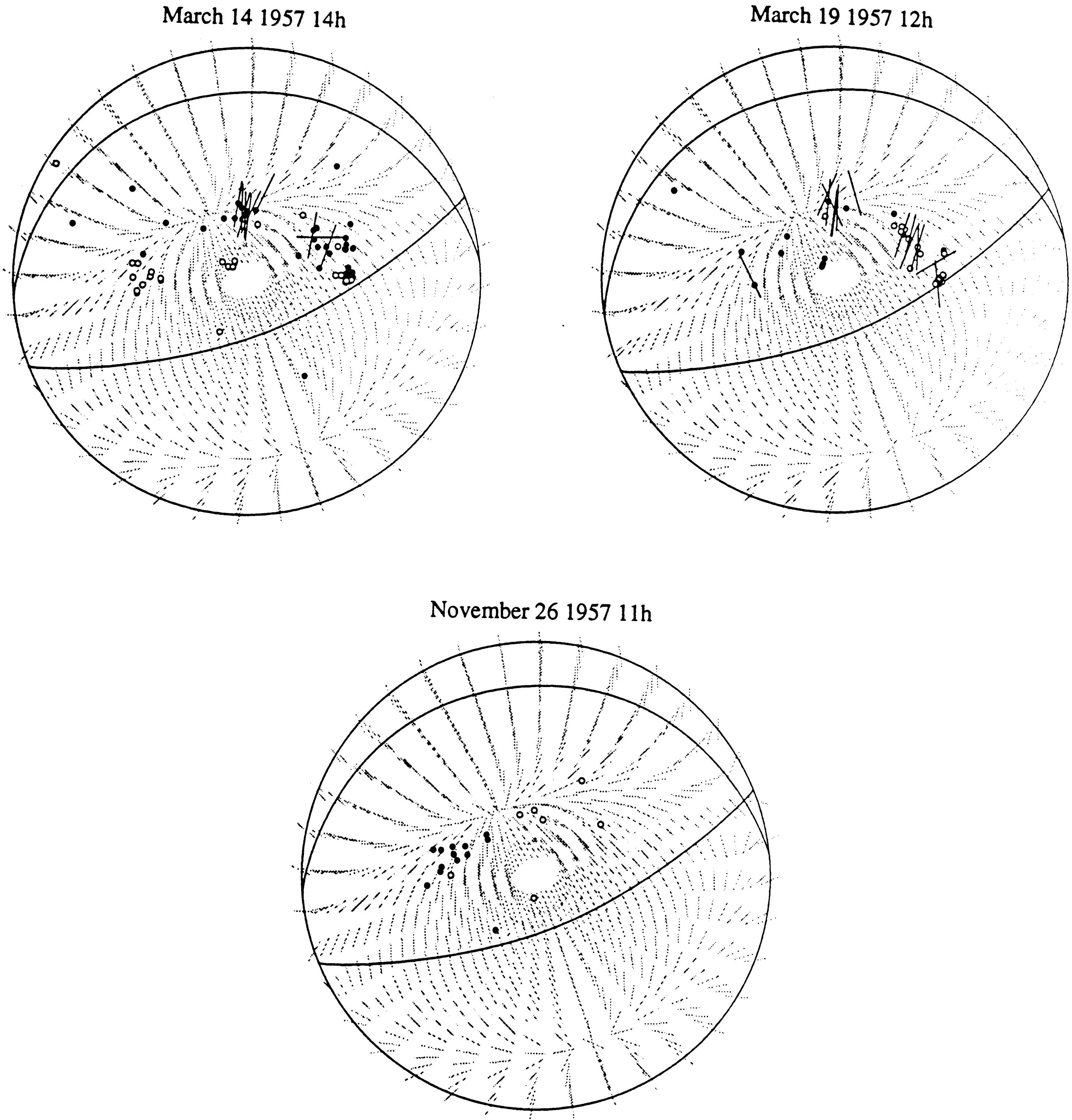

Figure 6: *P-wave* first motins and *S-wave* polarizations for events that do not appear to be either thrust or normal faulting earthquakes.

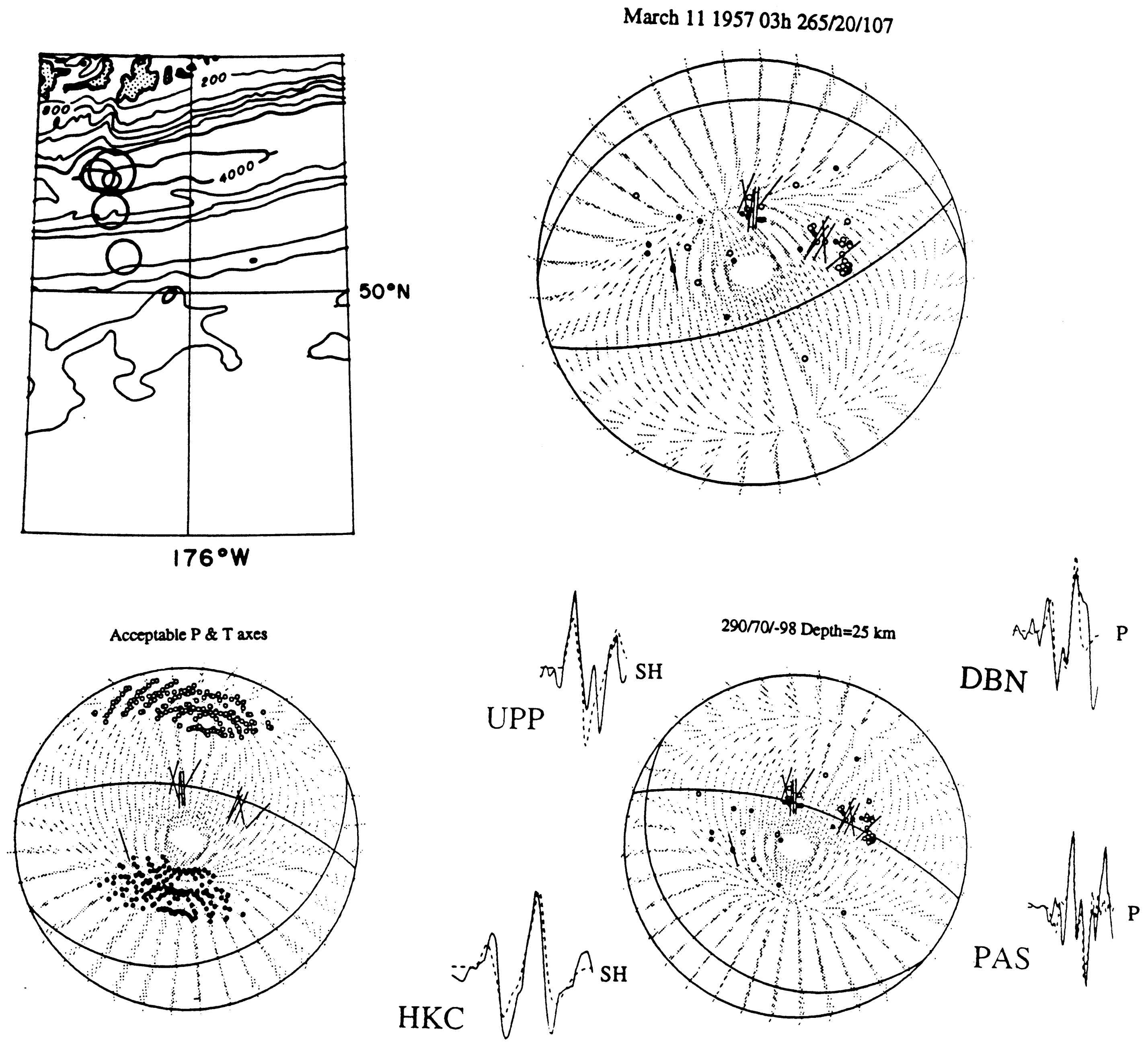

Figure 7: Source mechanism determination for and event in class 3. Map shows location of the event in question plus four of its aftershocks. Top focal sphere shows the observed first motions and polarization directions. Using the polarization directions the focal sphere to the left shows acceptable positions of the P and T axes. With this constraint, the focal sphere to the right shows the final source mechanism and several modeled waveforms.